Journal of Ginseng Research 47 (2023) 784–794

Contents lists available at ScienceDirect

Journal of Ginseng Research

journal homepage: https://www.sciencedirect.com/journal/journal-of-ginseng-research

Research Article

Ginsenoside Rg5 promotes wound healing in diabetes by reducing the negative regulation of SLC7A11 on the efferocytosis of dendritic cells

Wei Xia [a, 1], Zongdong Zhu [b, 1], Song Xiang [a, **], Yi Yang [a, *]

[a] Department of Endocrinology, Sichuan Provincial People's Hospital, School of Medicine, University of Electronic Science and Technology of China, Chengdu, China
[b] Department of Orthopedics, Sichuan Provincial People's Hospital, School of Medicine, University of Electronic Science and Technology of China, Chengdu, China

ARTICLE INFO

Article history:
Received 6 April 2023
Received in revised form
31 May 2023
Accepted 19 June 2023
Available online 30 June 2023

Keywords:
ginsenoside Rg5
SLC7A11
diabetes
wound healing

ABSTRACT

Background: ginsenoside Rg5 is a rare ginsenoside with known hypoglycemic effects in diabetic mice. This study aimed to explore the effects of ginsenoside Rg5 on skin wound-healing in the *Lepr*$^{db/db}$ mutant (*db/db*) mice (C57BL/KsJ background) model and the underlying mechanisms.
Methods: Seven-week-old male C57BL/6J, *SLC7A11*-knockout (KO), the littermate wild-type (WT), and *db/db* mice were used for *in vivo* and *ex vivo* studies.
Results: Ginsenoside Rg5 provided through oral gavage in *db/db* mice significantly alleviated the abundance of apoptotic cells in the wound areas and facilitated skin wound healing. 50 μM ginsenoside Rg5 treatment nearly doubled the efferocytotic capability of bone marrow-derived dendritic cells (BMDCs) from *db/db* mice. It also reduced NF-κB p65 and *SLC7A11* expression in the wounded areas of *db/db* mice dose-dependently. Ginsenoside Rg5 physically interacted with SLC7A11 and suppressed the cystine uptake and glutamate secretion of BMDCs from *db/db* and *SLC7A11*-WT mice but not in BMDCs from *SLC7A11*-KO mice. In BMDCs and conventional type 1 dendritic cells (cDC1s), ginsenoside Rg5 reduced their glycose storage and enhanced anaerobic glycolysis. Glycogen phosphorylase inhibitor CP-91149 almost abolished the effect of ginsenoside Rg5 on promoting efferocytosis. Conclusion: ginsenoside Rg5 can suppress the expression of SLC7A11 and inhibit its activity via physical binding. These effects collectively alleviate the negative regulations of SLC7A11 on anaerobic glycolysis, which fuels the efferocytosis of dendritic cells. Therefore, ginsenoside Rg5 has a potential adjuvant therapeutic reagent to support patients with wound-healing problems, such as diabetic foot ulcers.

1. Introduction

In patients with type I and type II diabetes mellitus (T1DM and T2DM), non-healing chronic wounds increase the risk of infection and seriously affect their life quality [1]. Tissue repair following skin wounds requires the clearance of apoptotic cells by phagocytes (a process known as efferocytosis) in the wounded areas [2]. Chronic and non-resolving inflammatory conditions in the wounded skin are associated with defects in efferocytosis [3–5].

Immune cells, including T cells, macrophages, neutrophils, and dendritic cells, cooperatively maintain the homeostasis of the skin microenvironment [6,7]. Resident or recruited dendritic cells, macrophages, and neutrophils can act as phagocytes in the skin, playing important roles in wound healing [8–10]. One recent study demonstrated that the membrane cystine/glutamate antiporter SLC7A11 serves as a negative regulator of efferocytosis in the wounded skin in diabetes, mainly via dendritic cells, but not macrophages [8]. Pharmacological inhibition of SLC7A11 function drastically accelerates wound healing in diabetic mice [8].

Ginsenosides are the main active ingredients of Panax ginseng Meyer. Previous studies showed some ginsenosides have anti-inflammatory and wound-healing-promoting effects, such as ginsenoside Rg1 [11], ginsenoside Rg3 [12], and ginsenoside Rh2 [13].

* Corresponding author. Department of endocrinology, Sichuan Provincial People's Hospital, School of Medicine, University of Electronic Science and Technology of China, Chengdu, 610072, China.
** Corresponding author. Department of endocrinology, Sichuan Provincial People's Hospital, School of Medicine, University of Electronic Science and Technology of China, Chengdu, 610072, China.
E-mail addresses: 342225310@qq.com (S. Xiang), spiritman2000@163.com (Y. Yang).
[1] Wei Xia and Zongdong Zhu contributed equally to this study.

https://doi.org/10.1016/j.jgr.2023.06.006

Ginsenoside Rg5 is a rare ginsenoside with known hypoglycemic effects that improve insulin resistance and mitochondrial biogenesis in diabetic mice [14,15]. In both *Lepr*$^{db/db}$ mutant (*db/db*) and high-fat diet/streptozotocin-induced diabetic mice, ginsenoside Rg5 suppresses the expression and activation of NF-κB p65 in liver and kidney tissues [14,16]. This suppressing effect was also observed in human keratinocytes and macrophages [17]. NF-κB p65 can activate *SLC7A11* transcription [18,19]. In addition, ginsenoside Rg5 might be an important skin care anti-aging ingredient of red ginseng [20]. Based on these clues, we hypothesized that ginsenoside Rg5 might generate beneficial effects on wound-healing in diabetes, probably through SLC7A11-mediated efferocytosis.

This study aimed to explore the effects of ginsenoside Rg5 on skin wound healing in the *db/db* mice model. In addition, we used *SLC7A11*-knock-out (KO) mice to study whether it affects SLC7A11-mediated efferocytosis of dendritic cells.

2. Materials and methods

2.1. Animal study

Seven-week-old male C57BL/6J, *SLC7A11*-KO, the littermate wild-type (WT), and the *db/db* mice (C57BL/KsJ background) were purchased from Cyagen Biosciences (Suzhou, China). Mice were housed under specific pathogen-free conditions in groups of two or three mice per cage. All animal procedures were approved by the Animal Care and Use Committee of Sichuan Provincial People's Hospital and Chengdu Jinruijie Biotechnology Service Center, China (Approval no. 202207006), following the Institutional Guidelines for the Care and Use of Animals. Following acclimatization (1 week), C57BL/6J or diabetic *db/db* mice (n = 6 per group) received the vehicle (0.5% (w/v) CMC-Na alone) or ginsenoside Rg5 (1.0 mg/mL, suspended in 0.5% (w/v) CMC-Na at 20 or 80 mg/kg/day) for one week via oral gavage before wounding.

Full-thickness wounds were made following the method as previously described [21]. Briefly, the mice were anesthetized using isoflurane. The back skin was shaved. Wounds were generated using 8-mm punch biopsy needles. The wound diameters (larger A and minor B) were measured every two days using a digital caliper. The wound area S was calculated using the flowing formula: $S = (A \times B \times \pi)/4$. The wounded tissues of representative mice at day 4 were collected after euthanasia using carbon dioxide (CO_2) inhalation. The tissues were fixed, embedded into paraffin, sectioned and subjected to hematoxylin and eosin (H&E) staining and immunofluorescent (IF) staining of cleaved caspase-3 (1:500, #9661, Cell Signaling Technology, Danvers, MA, USA).

2.2. Primary cell cultures

Bone marrow-derived dendritic cells (BMDCs) were generated from femurs and tibia of 8 to 12-week-old *db/db*, *SLC7A11*-WT or *SLC7A11*-KO mice via culturing bone marrow progenitors for 10-12 days in granulocyte-macrophage colony-stimulating factor (GM−CSF)−supplemented medium following the Lutz et al.'s method [22]. Bone marrow-derived macrophages (BMDMs) were generated following a method that uses both macrophage colony-stimulating factor (MCSF) and GM-CSF, as described previously [23]. After the induction, BMDCs were validated by FITC anti-mouse MHC-II (11-5321-82, Thermo Fisher Scientific, Waltham, MA, USA) and BV786 anti-mouse CD11c (cat#563735, BD Biosciences, Franklin Lakes, NJ, USA). In contrast, BMDMs were validated using PerCP/Cy5.5 anti-mouse F4/80 (cat#123127, Biolegend, Dedham, MA, USA) and BV510 Anti-mouse CD11b (cat#101245, Biolegend) by flow cytometry. Ginsenoside Rg5, erastin, cytochalasin D and CP-91149 were purchased from MedChemExpress (Monmouth Junction, NJ, USA).

2.3. Reverse transcription-quantitative real-time PCR (RT-qPCR)

Total RNA was reversely transcribed to cDNA. qPCR was conducted with an ABI PRISM 7900HT Sequence Detection System and SYBR Green Master Mix reagents (Applied Biosystems, Bedford, MA, USA). Gene expression was normalized to the expression of *PPIA* and calculated using the $2^{-\Delta\Delta CT}$ method. The following primers were used: mouse *SLC7A11*, forward, 5′-CTTTGTTGCCCTCTCCTGCTTC-3'; reverse, 5′- CAGAGGAGTGTGCTTGTGGACA-3'; mouse *PPIA*, forward, 5′-CATACAGGTCCTGGCATCTTGTC-3'; reverse, 5′-AGACCACATGC TTGCCATCCAG-3'.

2.4. Data retrieved from the human protein atlas

SLC7A11 RNA expression at the single-cell level in the normal human skin tissue was retrieved from the Human Protein Atlas (https://www.proteinatlas.org/) [24,25].

2.5. Western blotting

Western blotting was performed following the protocol introduced previously [26]. The wound kin tissues were homogenized in cell lysis buffer, with protease and phosphatase inhibitor cocktails (MilliporeSigma, St. Louis, MI, USA). The total protein extracts (20 μg) were separated with 10% SDS-PAGE and transferred to polyvinylidene difluoride membranes (MilliporeSigma). The membranes were washed, blocked, and were then incubated with diluted primary antibodies overnight at 4 °C. Then, they were thoroughly washed and incubated with horseradish peroxidase-linked (HRP) anti-rabbit IgG secondary antibody (Proteintech, Wuhan, China) for 1 h at room temperature. The protein signals were developed using an ECL reagent (BeyoECL Star, Beyotime, Shanghai, China) and Tanon 4600 Chemiluminescent Imaging System (Tanon, Shanghai, China). The following primary antibodies and dilutions were applied: anti−NF−κB p65 (1:1000, 10745-1-AP, Proteintech), anti-IκBα (1:5000, 10268-1-AP, Proteintech), anti-SLC7A11 (1:1000, 26864-1-AP, Proteintech), anti-β-actin (1:10000, 66009-1-Ig, Proteintech), anti-Histone H3 (1:2000, 17168-1-AP, Proteintech).

2.6. Cystine uptake and glutamate secretion assays

Sodium-independent cystine uptake was measured following the sodium nitroprusside-based assay introduced previously [27]. In brief, 5×10^5 BMDCs were seeded in 6-well plates. Cells were treated with ginsenoside Rg5 (10 μM or 50 μM for 48 h). Then, cells were washed, incubated with cystine uptake buffer, and then mixed with 1 μM L-cystine for 1 hr at 37°C. 500 ml uptake buffer was collected from each well and centrifuged. 400 μl of the supernatant was mixed with 100 μl of 20% sodium nitroprusside solution. Then, absorbance at 521 nm was measured. Glutamate secretion from the samples was measured using a Nova BioProfile 100 Plus Analyzer (Nova Biomedical, Waltham, MA, USA). Cystine and glutamate concentrations were calculated by subtracting from blank controls without cells and normalized to cell counts from each well.

2.7. In vitro engulfment, flow cytometric analysis, and cell sorting

Engulfment assay was performed following the methods introduced previously [28]. Jurkat cells have several advantages as a tool for efferocytosis assays, including rapid growth, consistent and

reproducible apoptosis induction, homogeneity, and relative simplicity [8,29–31]. In brief, human Jurkat T cells were treated with 254-nm UV lamp for 15 min, followed by incubation for 4 h at 37 °C with 5% CO_2. Apoptosis was verified by Annexin V-7AAD viability staining (cat#559763, BD Biosciences), by flow cytometric analysis. Apoptotic Jurkat cells were labeled with 1 μM CypHer5E (GE Healthcare, PA15401) for 30 min before use in the engulfment assays. Mouse BMDMs, BMDCs, conventional type 1 dendritic cells (cDC1s) or cDC2s were seeded in a 24-well plate. For drug treatment, BMDCs or cDCs were incubated with erastin (10 μM) or ginsenoside Rg5 (10 or 50 μM ginsenoside Rg5 for 2 h. Then, they were incubated with target apoptotic Jurkat cells at a 1:5 ratio for 2 h. Following the co-culture, cells were collected, washed 3 × with cold PBS and resuspended in FACS buffer. Then, FACS buffer is discarded. Dendritic cells were stained with FITC anti-mouse MHC-II (11-5321-82, Thermo Fisher Scientific) and BV786 anti-mouse CD11c (cat#563735, BD Biosciences), while BMDMs were stained with PerCP/Cy5.5 anti-mouse F4/80 (cat#123127) and BV510 Anti-mouse CD11b (cat#101245, Biolegend) diluted 1:200 in FACS buffer at 4°C for 30 min. Cells were analyzed on a BD FACS Canto II flow cytometer. Data analysis was carried out using NovoExpress software (v1.5.4, Agilent Technologies, Santa Clara, CA, USA). The efferocytotic index (phagocytosis) was calculated as follows: for dendritic cells, the CypHer5E+/CD11c+/MHC-II + cell-population was divided by the total CD11c+/MHC-II + cell count and multiplied by 100, while for BMDMs, the CypHer5E+/CD11b+/F4/80+ cell-population was divided by the total CD11b+/F4/80+ cell count and multiplied by 100.

To get primary cDC1s and cDC2s, mice spleen single-cell suspensions were prepared following the protocol introduced previously [8]. In brief, mice spleen tissues were digested and red blood cells were removed using a RBC lysis buffer (cat#420301, Biolegend). cDC1s and cDC2s were obtained by fluorescence-activated cell sorting, with BV650 anti-mouse/rat XCR1 (cat#148220, Biolegend) and APC anti-mouse CD172a (cat#144013, Biolegend). Cell sorting was performed using a BD FACSAria II flow cytometer.

2.8. Molecular docking

The ginsenoside Rg5 structure was transferred into a mol. file. The cryo-EM structure of the SLC7A11/SLC3A2 complex (https://www.rcsb.org/structure/7P9U) was downloaded and separated into two files containing SLC7A11 or SLC3A2 structure. Molecular docking was used for molecular docking using CB-Dock (http://clab.labshare.cn/cb-dock/php/index.php) [32].

2.9. Cellular thermal shift assay (CETSA)

CESTA was performed following a previously introduced method [33]. In brief, BMDCs were harvested with PBS buffer and lysed. Then, the cell lysates were mixed and incubated with DMSO (1%), Rg5 (50 μM) or erastin (10 μM) at room temperature for 30 min. The mixture samples were divided into aliquots and subjected to paralleled incubation at different temperatures ranging from 42 °C to 67 °C for 5 min. Then, the samples were centrifuged and used for western blotting to detect the presence of SLC7A11.

2.10. Surface plasmon resonance (SPR) analysis

The binding affinity of ginsenoside Rg5 to recombinant SLC7A11, SLC2A1, SLC7A5 and SLC16A1 proteins were measured using a Biacore T200 (GE Healthcare, Pittsburgh, PA, USA) and a CM5 sensor chip (carboxylated dextran surface) following the methods introduced previously [34]. Commercial recombinant SLC7A11, SLC2A1, SLC7A5, and SLC16A1 proteins were immobilized on the chip surface via amide linkages at pH 4.0. Ginsenoside Rg5 was serially diluted in the running buffer (pH7.4, HBS-P+ (HBS, 0.05% Tween20)) and flowed over the CM5 chip with immobilized proteins to record resonance changes. Data transformation, overlay plots, and interaction analysis were prepared with BIAevaluation 3.2 software (Cytiva, Marlborough, MA, USA). The kinetic constants were used to calculate the dissociation constant (K_D).

2.11. Measurement of glycogen concentration

The glycogen concentration was quantified using a Glycogen Assay Kit (ab65620, Abcam, Cambridge, UK).

2.12. Seahorse analysis

BMDCs were analyzed by Seahorse XFe96 Analyzer (Agilent Technologies) to measure ECAR in real-time. In brief, cells (5×10^4 cells/well) were seeded on a Seahorse 96-well tissue culture plate (Agilent Technologies). The plates were incubated in a cell incubator overnight before analysis. Then, the cells were treated with 10 μM erastin or 50 μM ginsenoside Rg5 2 h before Seahorse analysis. Then, the medium was changed to unbuffered, glucose-free DMEM supplemented with 2 mM glutamine. Seahorse XF Glycolysis Stress Test Kit (103020-100, Agilent Technologies) was used following the manufacturer's instructions. Measurements from the assay were then normalized to cell numbers.

2.13. Statistical analysis

Data presented as mean ± standard deviation (SD). One-way ANOVA with Turkey post hoc tests was used for analyses as indicated, while unpaired Welch's T-test was conducted for two-group comparisons. GraphPad Prism 8.1.0 (GraphPad Software, La Jolla, CA, USA) was used for statistical analysis. $P < 0.05$ was considered significant.

3. Results

3.1. Ginsenoside Rg5 promotes wound healing in the skin of diabetic mice

Since ginsenoside Rg5 (Fig. 1A) has a known hypoglycemic effect and can improve insulin resistance in diabetic mouse models [14,15], we tested whether it facilitates wound healing in the leptin receptor-deficient *db/db* mice compared to C57BL/6J mice. This experimental model mimics human type 2 diabetes with obesity and hyperglycemia. The experimental design is summarized in Fig. 1B. C57BL/6J and *db/db* mice received vesicle or ginsenoside Rg5 (20 mg/kg or 80 mg/kg) for one week via oral gavage before wounding (Fig. 1B). The skin excision experiment indicated that compared to C57BL/6J mice, wound healing was delayed in *db/db* mice. However, both C57BL/6J and *db/db* mice had significantly facilitated wound healing (Fig. 1C and D). *db/db* mice administrated with 80 mg/kg ginsenoside Rg5 reached the half-maximal closure approximately two days earlier than the vehicle control (Fig. 1E and F).

Uncleared apoptotic cells in the wound areas are an important cause of chronic inflammation and delayed wound healing [35]. Therefore, we checked apoptotic and cleaved caspase-3 positive cells in the wound areas by IF staining. Results showed that ginsenoside Rg5 treatment drastically alleviated the apoptotic cell burden in the wound areas, with fewer unclear cleaved caspase-3 positive cells in both C57BL/6J and *db/db* mice (Fig. 1G and H). Wounds of C57BL/6J mice without ginsenoside Rg5 treatment had around 400 apoptotic cells (mean ± SD, 424 ± 93/cm) at day 4 post-

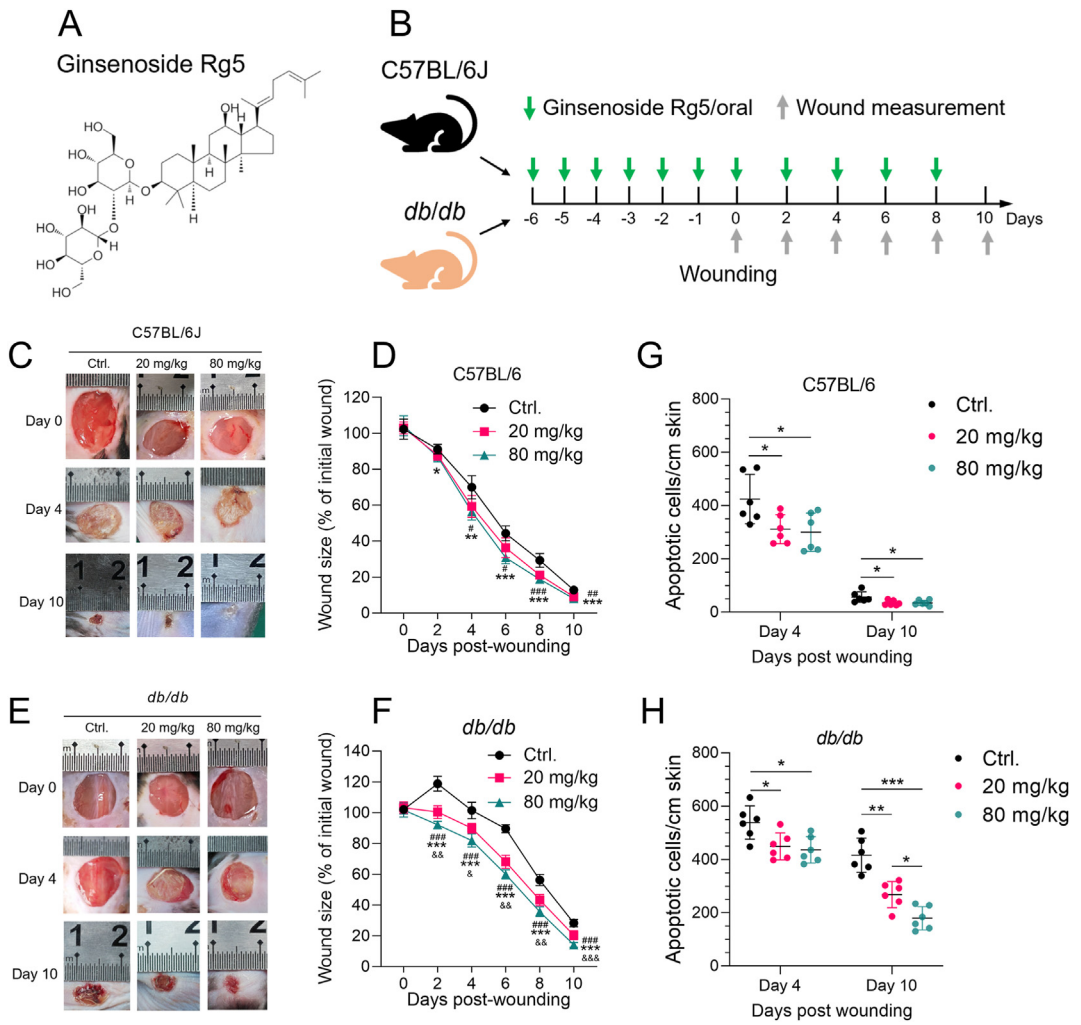

Fig. 1. Ginsenoside Rg5 promotes wound healing in the skin of diabetic mice. **A.** The chemical structure of ginsenoside Rg5. **B.** A schematic map showing the experimental design. **C**–**F.** Representative images of wounds at different time points (C and E) and quantitative wound healing dynamics of C57BL/BJ (C-D) and *db/db* (E-F) mice treated vesicle control or ginsenoside Rg5 from day 0 to day 10 (n = 6 per group). Data representative of 3 independent experiments. **G-H.** Quantification of apoptotic cells (defined as cleaved caspase-3 positive) per cm skin in the wounded skin from C57BL/BJ (G) and *db/db* (H) mice treated vesicle control or ginsenoside Rg5 at day 4 after wounding was performed (n = 3). One-way ANOVA with Tukey multiple comparison tests was performed. # comparison between 20 mg/kg and control groups; * comparison between 80 mg/kg and control groups; & comparison between 20 mg/kg and 80 mg/kg groups; *,# and &, $p < 0.01$; **, ## and &&, $p < 0.01$; ***, ### and &&&, $p < 0.001$.

wounding and around 60 apoptotic cells (mean ± SD, 57 ± 20/cm) at day 4 post wounding (Fig. 1G). In the 80 mg/kg ginsenoside Rg5 treatment group, the numbers decreased to 300 ± 72 and 35 ± 10 per cm at the two time points (Fig. 1G). In *db/db* mice without ginsenoside Rg5 treatment, the number of apoptotic cells per cm at day 4 and 10 post-wounding were 539 ± 63 and 416 ± 64 per cm (Fig. 1H). In 80 mg/kg ginsenoside Rg5 treated *db/db* mice, the numbers dropped to 437 ± 50 and 179 ± 44 per cm at the two time points (Fig. 1H).

3.2. Ginsenoside Rg5 enhances the efferocytosis of BMDCs in diabetic mice

Considering the significantly decreased apoptotic cells, we hypothesized that efferocytosis might play a part in the process. Since macrophages and dendritic cells are two main types of professional phagocytes [2], we prepared primary BMDMs and BMDCs from bone marrow progenitors from C57BL/6J and *db/db* mice and confirmed successful induction using macrophage markers (F4/80 and CD11b) and dendritic cell markers (MHC-II and CD11c) by flow cytometry (Fig. 2A). Then, we tested how ginsenoside Rg5 affected their efferocytotic capability by flow cytometry. BMDMs and BMDCs were with CypHer5E-labeled apoptotic cells at a ratio of 5:1 for 2 h. Then, the percentage of CypHer5E + events within the CD11b+ and F4/80+ BMDMs and within the CD11C+ and MHC-II + BMDCs were quantified by flow cytometry (Fig. 2B). Results showed that BMDMs and BMDCs from *db/db* mice had decreased efferocytosis compared to the counterparts from wild-type mice (Fig. 2C). Ginsenoside Rg5 significantly enhanced the efferocytotic capability of BMDMs and BMDCs from *db/db* mice. However, this trend was more evident in BMDCs (Fig. 2D). 50 μM ginsenoside Rg5 treatment nearly doubled the efferocytotic capability of BMDCs from *db/db* mice. In contrast, it did not enhance the uptake of live cells of BMDCs (Fig. 2D). Therefore, our subsequent studies focused on the potential regulatory effects of ginsenoside Rg5 on BMDCs.

43.3. Ginsenoside Rg5 suppresses SLC7A11 expression in BMDCs from db/db mice

One recent study indicated that the expression of *SLC7A11* was about 200-fold higher in the wounds of *db/db* mice than in WT C57BL/6J mice [8]. The drastically upregulated *SLC7A11* was verified

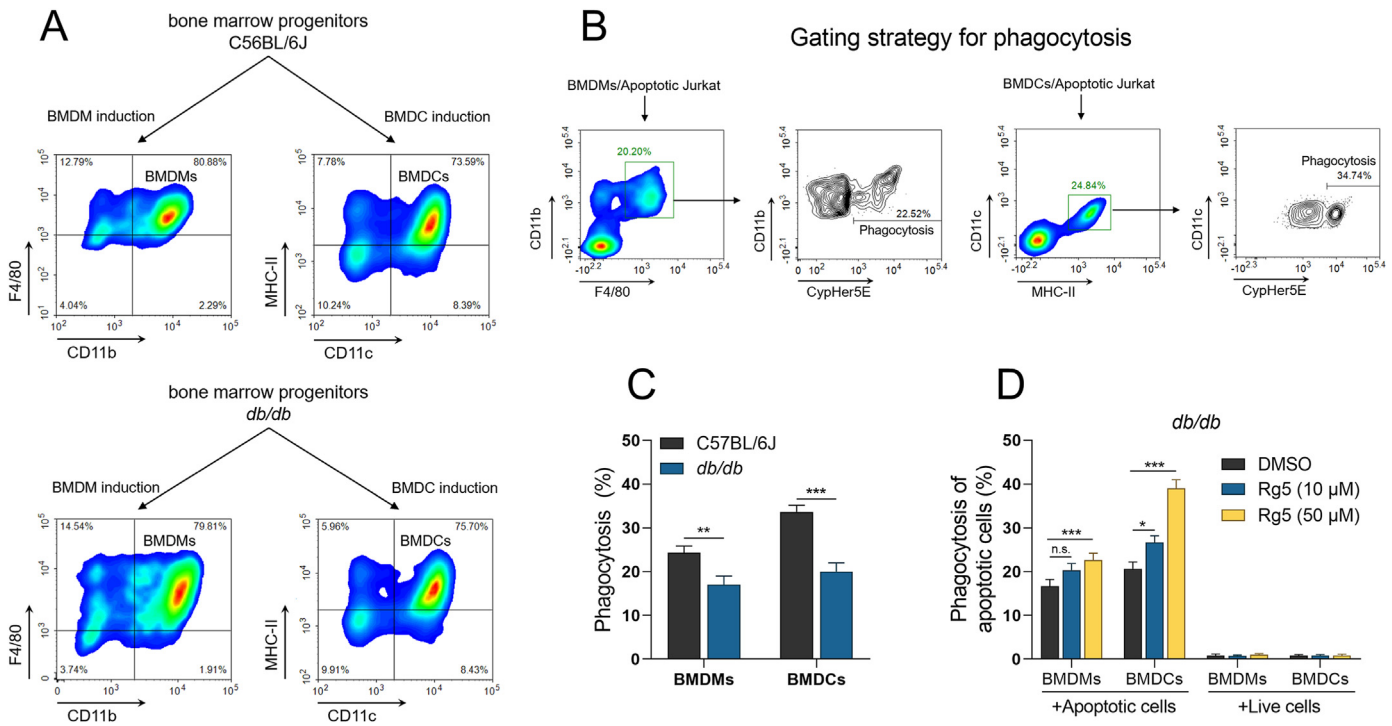

Fig. 2. Ginsenoside Rg5 enhances the efferocytosis of bone marrow-derived dendritic cells (BMDCs) from diabetic mice. **A.** Representative flowcytometric analysis to confirm the successful induction of BMDMs and BMDCs from bone marrow progenitors from C57BL/6J and *db/db* mice, respectively, using macrophage markers (F4/80 and CD11b) and dendritic cell markers (MHC-II and CD11c). **B.** Gating strategy to identify phagocytosis. BMDMs and BMDCs were co-cultured with CypHer5E-labeled apoptotic or live Jurkat cells at a ratio of 5:1 for 2 h. Then, the percentage of CypHer5E + events within the CD11b+ and F4/80+ BMDMs and within the CD11C+ and MHC-II + BMDCs were quantified by flow-cytometry. **C.** Statistical comparison of the difference in the efferocytotic capability of BMDMs and BMDCs derived from C57BL/6J and *db/db* mice. **E.** Effect of ginsenoside Rg5 on efferocytosis of BMDMs and BMDCs derived from *db/db* mice. Data from at least 3 independent experiments with 3 replicates. Data are mean ± SD. One-way ANOVA with Tukey multiple comparison tests was performed. *, $p < 0.01$; **, $p < 0.01$; ***, $p < 0.001$; n.s., not significant.

in our mice models (Fig. 3A). Then, we checked whether ginsenoside Rg5 treatment altered *SLC7A11* expression. Results showed that ginsenoside Rg5 treatment substantially suppressed *SLC7A11* expression in the wounds of *db/db* mice at the mRNA and protein levels at day 4 post-wounding, compared to normoglycaemic C57BL/6J mice (Fig. 3A–B, E). Besides, it suppressed total NF-κB p65 and restored IκBα expression in the wound tissue in a dose-dependent manner (Fig. 3B–D). In addition, it suppressed the nucleus entrance of p65 (Fig. 3B and F). By checking the single-cell RNA-seq data in normal human skin in the Human Protein Atlas, we found that *SLC7A11* mainly expressed in Lagnerhams cell (a specialized macrophage-DC hybrid population) [36], macrophages and B-cells (Fig. 3G).

3.4. Ginsenoside Rg5 interacts with SLC7A11 with a high affinity and suppresses its cystine/glutamate antiporter activity

Some ginsenosides could interact with and be transported via certain solute carrier members [37–39]. We conducted a molecular docking assay to visualize the potential interaction between ginsenoside Rg5 and SLC7A11 (Fig. 4A and B). Interestingly, the Vina score of the best docking model is low (−9.4 kcal/Mol). The model of the ginsenoside Rg5-binding pocket is located in the intracellular vestibule of SLC7A11, which is similar to erastin, a known inhibitor of SLC7A11 [40]. It is known that Q191, F254, and F336 are critical for the cystine uptake capability of SLC7A11 [40]. In the predicted binding model, ginsenoside Rg5 might directly interact with F336 (Fig. 3B, green arrows), and several residues close to F254 (F250, Y251, L252, and N253) (Fig. 4B, green circle). Cystine uptake via SLC7A11 can suppress efferocytosis [8]. Therefore, we tested the binding between ginsenoside Rg5 and multiple SLC family members with known regulatory effects on efferocytosis, including SLC7A11, SLC2A1, SLC7A5, and SLC16A1 [8,29]. SPR results confirmed a high binding affinity of ginsenoside Rg5 to SLC7A11 ($K_D = 0.82 \pm 0.16$ μM) and SLC2A1 ($K_D = 0.59 \pm 0.11$ μM) (Fig. 4C). The following CETSA data indicated that ginsenoside Rg5 increased the thermostability of SLC7A11 but not β-actin protein in BMDCs from *db/db* mice (Fig. 4D–F).

After that, we compared how ginsenoside Rg5 affected cystine uptake and glutamate secretion of BMDCs from *db/db*, genetic *SLC7A11*-deficient (*SLC7A11*-KO), and *SLC7A11* wild-type (*SLC7A11*-WT) mice (Fig. 4G). Results showed that like erastin, ginsenoside Rg5 suppressed cystine uptake and glutamate secretion of BMDCs from *db/db* and *SLC7A11*-WT mice (Fig. 4H–I, K-L). However, these regulations were not observed in BMDCs from *SLC7A11*-KO mice (Fig. 4J and M).

3.5. Ginsenoside Rg5 treatment enhances the efferocytosis of dendritic cells

Ginsenoside Rg5 substantially enhanced the efferocytotic capability of BMDCs from *SLC7A11*-WT mice, similar to the effect of erastin (Fig. 5A). This effect was canceled via interrupting cytoskeletal rearrangement with cytochalasin D (CytoD) (Fig. 5A). In comparison, it only slightly elevated the efferocytosis of BMDCs from *SLC7A11*-KO mice (Fig. 5A). Due to different gene expression profiles, *in vitro* BMDCs might not fully reflect conventional DCs (cDCs) [41,42]. Through cell sorting, we purified cDCs from SLC7A11-WT and -KO mice (Fig. 5B). Ginsenoside Rg5 enhanced the efferocytosis of cDC1s (Fig. 5C), but not cDC2s from *SLC7A11*-WT

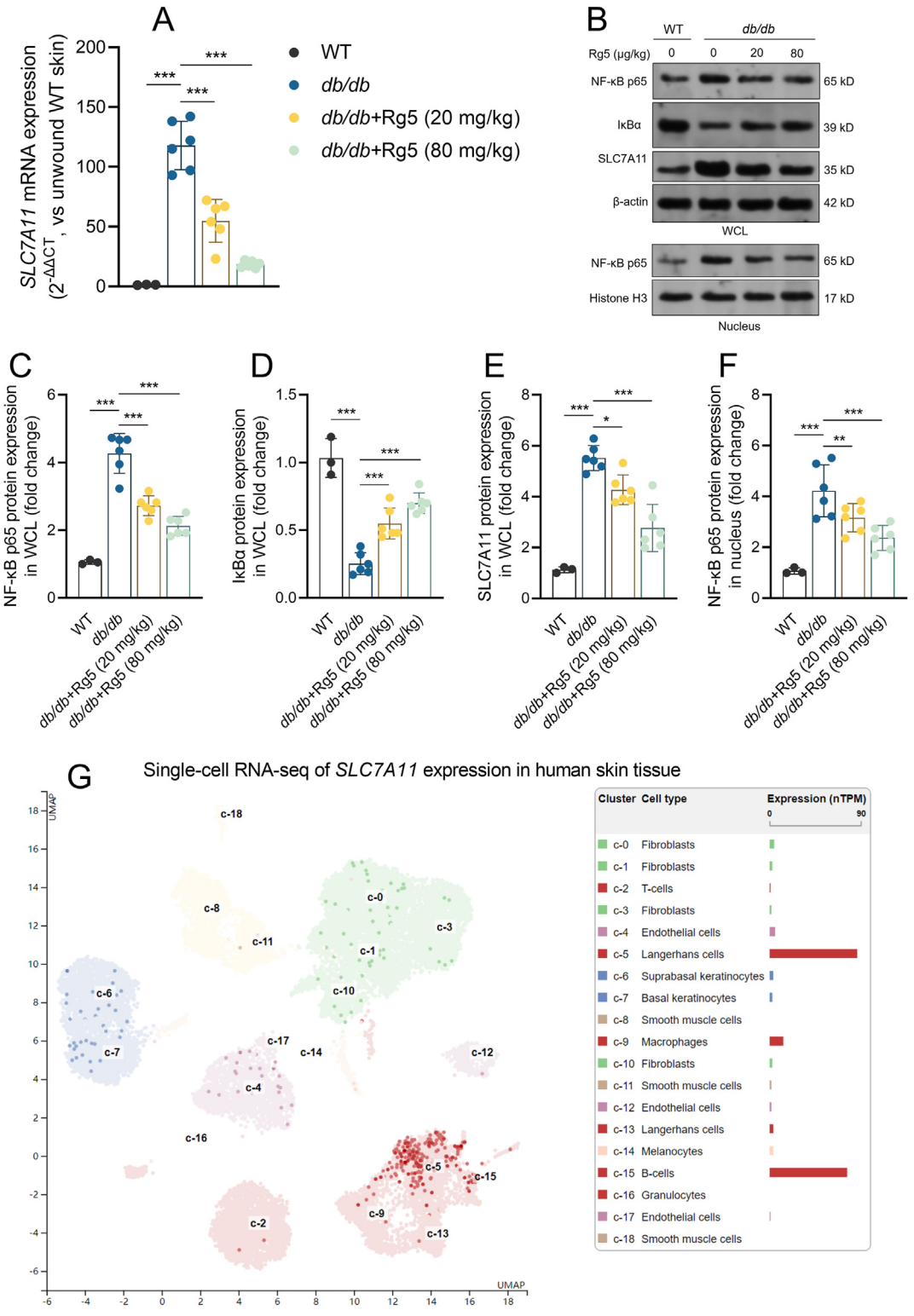

Fig. 3. Ginsenoside Rg5 suppresses *SLC7A11* expression in BMDCs from *db/db* mice. **A.** qRT-PCR was conducted to quantify *SLC7A11* expression in skin lysates from unwounded wild-type (n = 3), wounded (day 4 after wounding) *db/db* mice (n = 6 per group) with or without ginsenoside Rg5 treatment (20 or 80 mg/kg). **B**–**F.** Representative images (B) and quantitation (C–F) of western blotting analysis to detect NF-κB, IκBA, and SLC7A11 expression in the whole cell lysate (WCL) or the nucleus part of the skin from unwounded wild-type (n = 3), wounded (day 4 after wounding) *db/db* mice (n = 6 per group) with or without ginsenoside Rg5 treatment (20 or 80 mg/kg). **G.** A UMAP plot (left) and a bar chart (right) showing *SLC7A11* RNA expression at the single-cell level in normal human skin tissue. Each dot corresponds to a cell in the UMAP lot. The right bar char shows RNA expression level (nTPM) in each cell type cluster. Data was obtained from v21, the Human Protein Atlas: via https://www.proteinatlas.org/ENSG00000151012-SLC7A11/single+cell+type/skin. Data are mean ± SD. One-way ANOVA with Tukey multiple comparison tests was performed. **, $p < 0.01$; ***, $p < 0.001$.

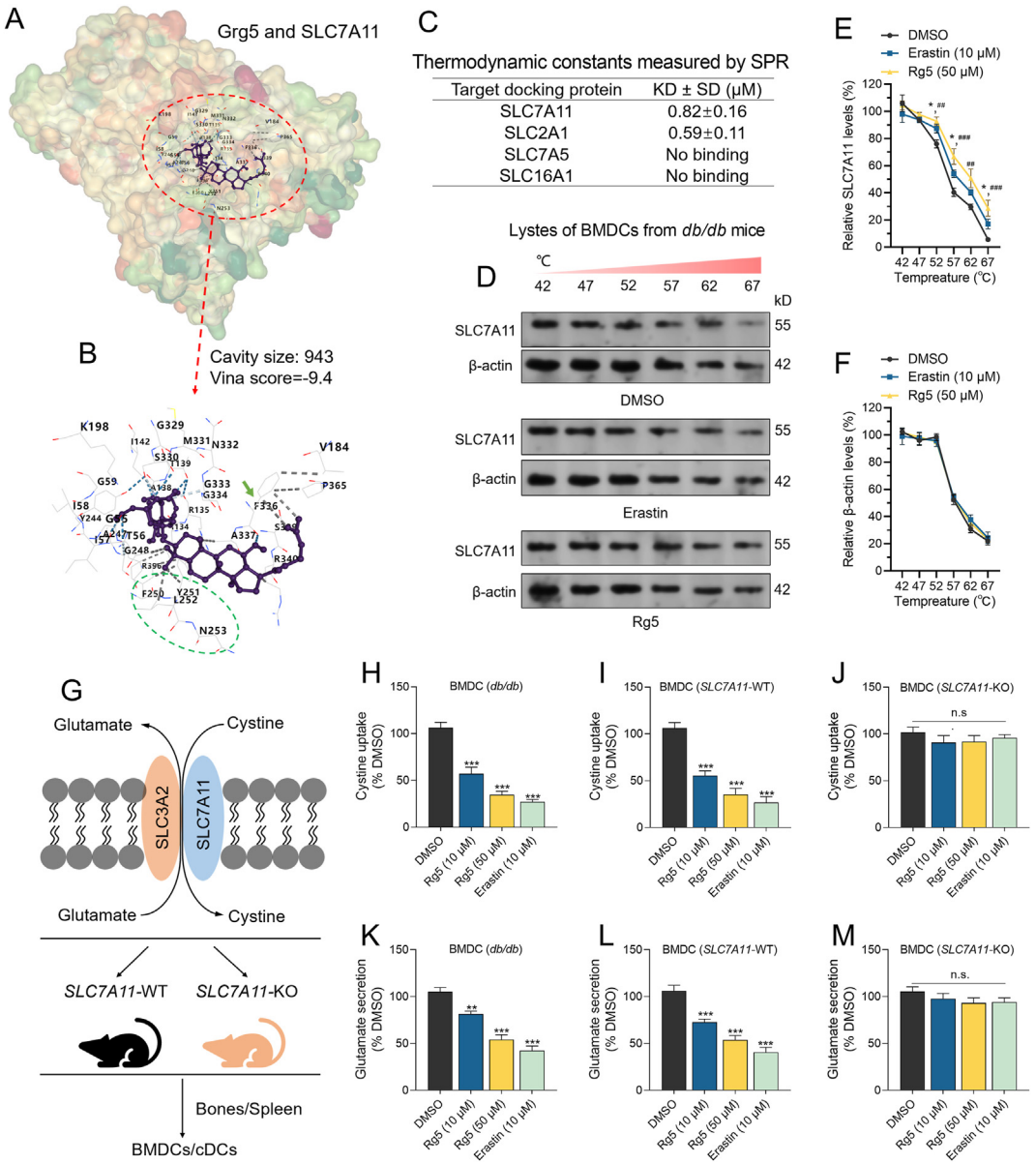

Fig. 4. Ginsenoside Rg5 interacts with SLC7A11 with a high affinity and suppresses its cystine/glutamate antiporter activity. A-B. The predicted binding position of ginsenoside Rg5 in SLC7A11 protein. Amino acid residues refer to the SLC7A11 protein. The detailed binding position was provided in panel B. **C.** Thermodynamic constants measured by SPR for the interaction between ginsenoside Rg5 and immobilized SLC proteins, including SLC7A11, SLC2A1, SLC7A5, and SLC16A1. **D-F.** Representative images (D) and quantitation (E-F) of CETSA. CETSA was conducted using cellular lysates of BMDCs from *db/db* mice, in the presence of DMSO (1%), 50 μM ginsenoside Rg5, or 10 μM erastin. β-actin expression served as a negative control. *, compassion between DMSO and erastin groups; #, compassion between DMSO and ginsenoside Rg5 groups. **G.** Schematic of SLC7A11 transport activity and the knockout mice used. **H-M.** Relative cystine uptake levels (H-J) and glutamate secretion levels (K-M) were measured to assess the influence of ginsenoside Rg5 (10 μM or 50 μM for 2 h) or erastin (10 μM for 2 h) pre-treatment on the cystine/glutamate antiporter activity of BMDCs from *db/db*, *SLC7A11*-WT and *SLC7A11*-KO mice. The mean ± SD is shown, n = 3. Statistical significance was determined using one-way ANOVA with Tukey's post hoc tests. *$p < 0.05$; *** and ###, $p < 0.01$; *** and ###, $p < 0.001$.

mice (Fig. 5C and D). Although ginsenoside Rg5 treatment showed a trend to elevate the efferocytosis of cDC1s from *SLC7A11*-KO mice, it did not reach a statistically significant level (Fig. 5C).

3.6. Ginsenoside Rg5 promotes DC efferocytosis via promoting SLC7A11-mediated anaerobic glycolysis

SLC7A11 inhibition can enhance DC efferocytosis via glycogenolysis [8]. Ginsenoside Rg5 treatment decreased intracellular glycogen of both BMDCs and cDC1s from *SLC7A11*-WT mice but not the counterparts from *SLC7A11*-KO mice (Fig. 6A and B). CP-91149 (a glycogen phosphorylase inhibitor) restored glycogen levels in ginsenoside Rg5-treated BMDCs and cDC1s (Fig. 6A and B). In addition, CP-91149 significantly weakened ginsenoside Rg5-dependent elevation in efferocytosis (Fig. 6C and D), suggesting that ginsenoside Rg5-mediated glycogenolysis is a major cause of enhanced DC efferocytosis.

To validate the influence of ginsenoside Rg5 on the anaerobic glycolysis of dendritic cells, we conducted a glycolysis stress test on BMDCs (from *SLC7A11*-WT or *SLC7A11*-KO mice) with or without pre-treatment of ginsenoside Rg5, using a Seahorse XFe96 Analyzer. Glucose, oligomycin, and 2-deoxyglucose (2-DG) were sequentially added. Non-glycolytic ECAR (before glucose addition) was not different among the groups (Fig. 6E and F). Ginsenoside

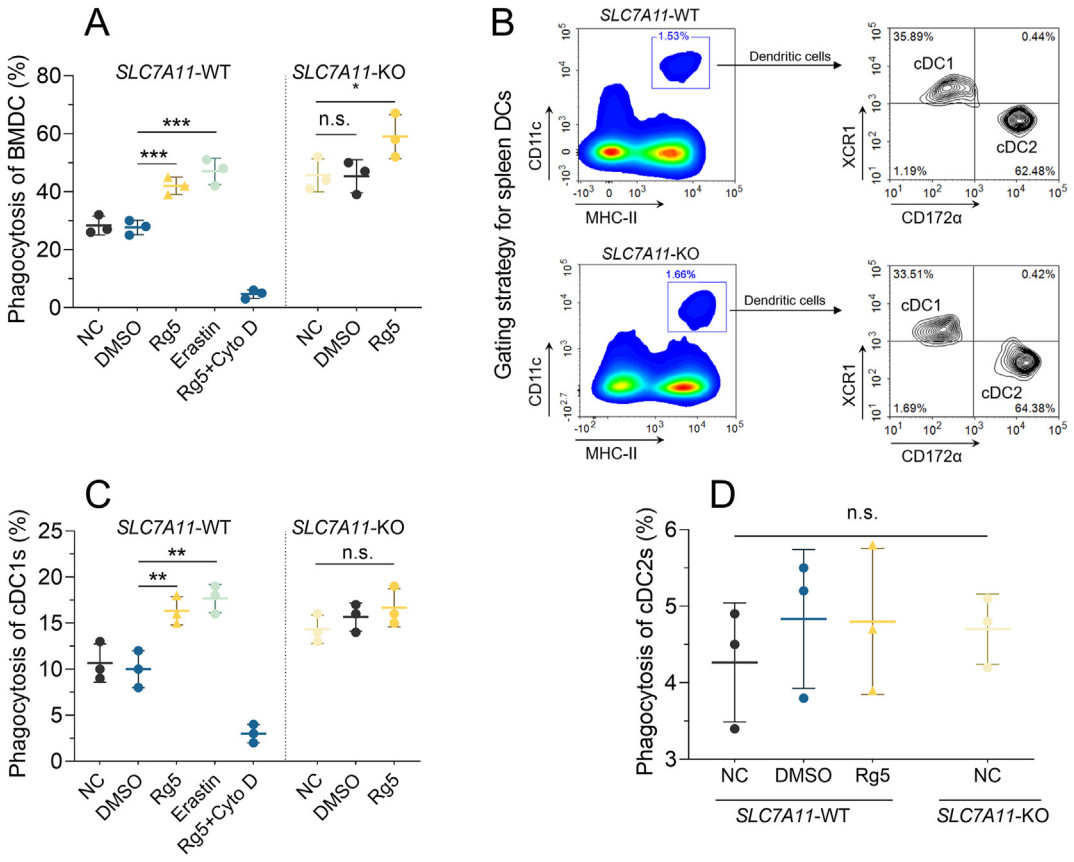

Fig. 5. Ginsenoside Rg5 treatment enhances the efferocytosis of dendritic cells. **A.** The effect of ginsenoside Rg5 treatment (50 μM, 2 h) on the efferocytosis of BMDCs from *SLC7A11*-KO or -WT mice. Phagocytosis was tested using CypHer5E-labelled apoptotic Jurkat cells at a 1:5 phagocyte: target ratio. Erastin was used as a positive control. **B.** Gating strategy to collect CDCs from the spleen tissue of 8-week *SLC7A11*-KO or -WT mice. **C-D.** Purified cDC1 (C) and cDC2 (D) subsets were tested for phagocytosis with apoptotic and live Jurkat cells for 4 h, with or without pre-treatment of ginsenoside Rg5 or erastin as indicated in panel A. Data were from 3 biological replicates. One-way ANOVA with Tukey multiple comparison tests was performed. *, $p < 0.01$; **, $p < 0.01$; ***, $p < 0.001$; n.s., not significant.

Rg5 or erastin treatment increased basal ECAR (elevated glycolysis) of BMDCs from *SLC7A11*-WT mice (Fig. 6E and G). We also found that BMDCs from *SLC7A11*-WT mice treated with ginsenoside Rg5 or erastin have increased glycolytic capacity, measured by the maximal ECAR after the addition of oligomycin, which inhibits mitochondrial respiration (Fig. 6E and H).

4. Discussion

Chronic non-healing wounds are a common complication of diabetes, which drastically increases the risk of infection and tissue necrosis. However, current therapeutic strategies are still limited due to a poor understanding of the underlying pathological mechanisms [43]. Some recent studies indicated that the high efficient efferocytosis supports wound healing [44,45]. Defects in efferocytosis mediated by macrophages and dendritic cells in the wound skin led to the accumulation of apoptotic cells and subsequent chronic inflammation [8,9,45]. In this study, we observed that ginsenoside Rg5 provided through oral gavage in *db/db* mice significantly alleviated the apoptotic cell burden in the wound areas and facilitated skin wound healing. 50 μM ginsenoside Rg5 treatment nearly doubled the efferocytotic capability of BMDCs from *db/db* mice. These findings suggest that ginsenoside Rg5 could facilitate wound healing by activating dendritic cell-mediated efferocytosis.

It is known that ginsenoside Rg5 can suppress the expression and activation of NF-κB p65 in multiple types of tissues, including human keratinocytes and macrophages [14,16,17]. NF-κB p65 serves as an activator of *SLC7A11* transcription [18,19], which is a molecular brake on efferocytosis of dendritic cells [8]. In this study, we confirmed that ginsenoside Rg5 treatment reduced NF-κB p65 and *SLC7A11* expression in the wounded areas of *db/db* mice dose-dependently. In addition, SLC7A11 expression could also be activated by nuclear factor erythroid-2 (NRF2) and the phosphorylated signal transducer and activator of transcription 3 (p-STAT3) [46,47]. Ginsenoside Rg5 can suppress NRF2 and STAT3 expression [48,49]. These mechanisms also partially explained the suppressive effect of ginsenoside Rg5 on *SLC7A11* transcription in the wounded areas.

Some ginsenoside might interact with SLC family members and affect their physiological functions. For example, ginsenoside Rg3 can interact with SLC2A1 [34], while ginsenoside Rd may interact with SLC5A1 [39]. In the current study, our molecular docking and subsequent SPR and CETSA assays validated the physical binding of ginsenoside Rg5 to SLC7A11, with a similar binding configuration to erastin. It is known that erastin may bind to the extracellular domain of SLC7A11 and induce conformational changes that prevent cystine uptake [40]. Like erastin, ginsenoside Rg5 might bind to multiple amino acid residuals of SLC7A11 that are critical for the cystine uptake activity, including F250, Y251, L252, N253, and F336 [40]. Reduced cystine uptake and increased glutamate secretion after SLC7A11 inhibition can lead to reactive oxygen species (ROS) accumulation. This mechanism partially contributes to enhanced efferocytosis of DCs [8]. Ginsenoside Rg5 drastically suppressed cystine uptake and glutamate secretion of BMDCs from *db/db* and

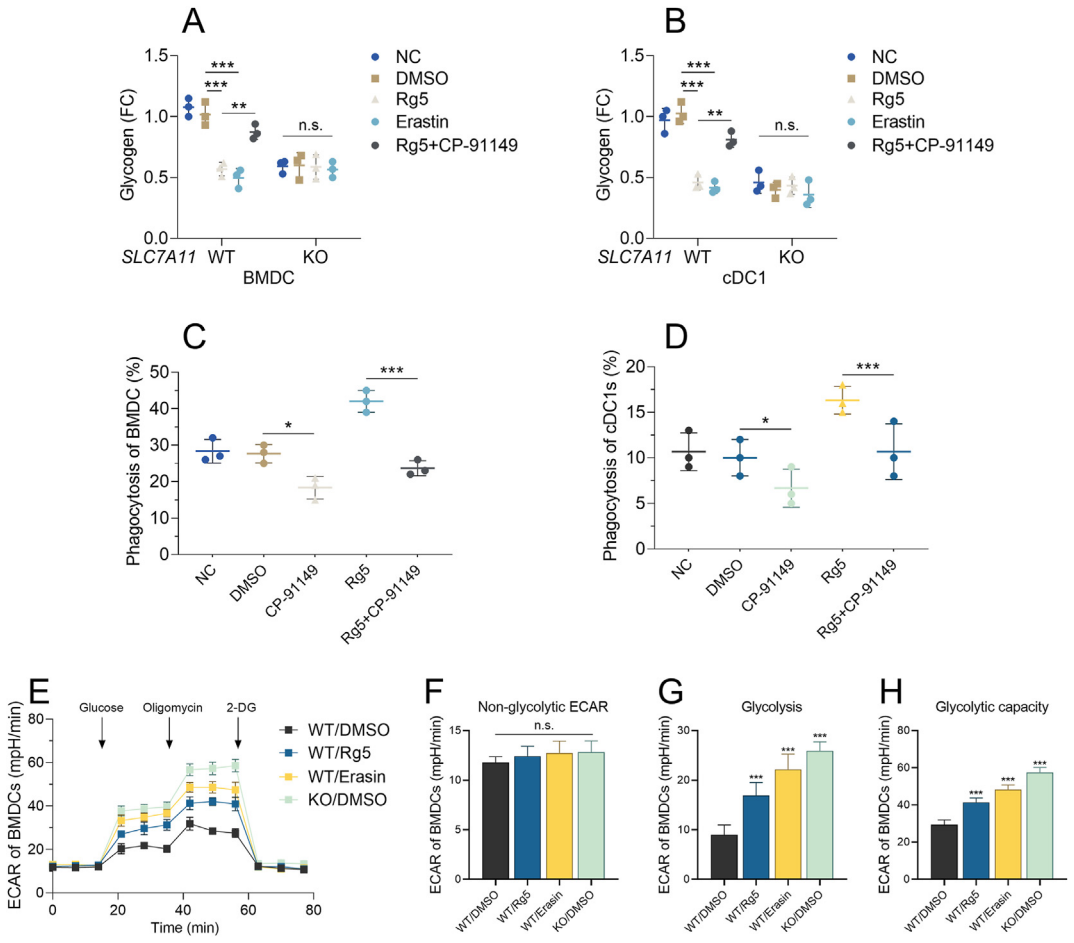

Fig. 6. Ginsenoside Rg5 promotes dendritic cell efferocytosis via promoting SLC7A11-mediated glycolysis. **A-D.** Glycogen levels in lysates (A-B) and efferocytosis (C-D) of BMDCs (A and C) or cDC1s (B and D) populations from *SLC7A1*1-WT or *SLC7A11*-KO mice, treated by DMSO, ginsenoside Rg5 or Erasin, or by combined ginsenoside Rg5 and CP-91149. **E-H.** ECAR was measured in the BMDCs from *SLC7A1*1-WT (WT) or *SLC7A11*-KO (KO) mice with indicated treatment over time with sequential treatments with glucose, oligomycin, and 2-deoxyglucose (2-DG). From this graph (E), non-glycolytic ECAR (ECAR before glucose addition) (F), glycolysis (difference between ECAR after glucose addition and non-glycolytic ECAR) (G) and glycolytic capacity (maximal ECAR after oligomycin treatment) (H) were determined. Data are mean ± SD of n = 3 per group. Statistical significance was determined using One-way ANOVA with Tukey multiple comparison tests. *, $p < 0.01$; **, $p < 0.01$; ***, $p < 0.001$; n.s., not significant.

*SLC7A1*1-WT mice but not in BMDCs from *SLC7A11*-KO mice. These findings imply that ginsenoside Rg5 could bind to SLC7A11 and suppress its cystine/glutamate antiporter activity. Therefore, we infer that ginsenoside Rg5 can enhance efferocytosis of dendritic cells via reducing *SLC7A11* transcription and inhibiting its cystine/glutamate antiporter activity. However, future mutational studies are required to validate the binding of ginsenoside Rg5 to the critical residues modulating the cystine uptake activity of SLC7A11.

Aerobic glycolysis plays a crucial role during the initiation and ongoing process of efferocytosis [29]. Dendritic cells have abundant intracellular glycogen reserves. Inhibition of SLC7A11 significantly increases anaerobic glycolysis, which fuels DC efferocytosis [8]. In BMDCs and cDC1s, we confirmed that ginsenoside Rg5 reduced their glycose storage and enhanced anaerobic glycolysis. Glycogen phosphorylase inhibitor CP-91149 nearly abolished the effect of ginsenoside Rg5 on promoting efferocytosis. Based on these findings, we infer that ginsenoside Rg5 can promote the efferocytosis of dendritic cells by abrogating the suppressive effect of SLC7A11 on glycolysis.

Ginsenoside Rg5 could enhance the efferocytotic capability of BMDMs from *db/db* mice (Fig. 2D). Thus, it might exert wound-healing effects through mechanisms other than SLC7A11-mediated efferocytosis of dendritic cells. In addition, in the current study, we found that Rg5 could alleviate the accumulation of NF-kB p65. Inhibiting Sprouty2 (Spry2) can enhance the efferocytosis of macrophages *in vitro* partially via decreasing NF-kB p65 phosphorylation [50]. Induction of glycogenolysis might not be the only reason for ginsenoside Rg5 action on efferocytosis. Besides SLC7A11, we observed that SLC2A1 is a potential docking protein of ginsenoside Rg5. Efferocytosis induces a novel SLC program to promote glucose uptake and aerobic glycolysis in phagocytes, initiated by SLC2A1-mediated glucose uptake, with concurrent suppression of the oxidative phosphorylation program [29]. Therefore, SLC2A1 is involved in metabolic changes during efferocytosis [29]. Therefore, ginsenoside Rg5 might participate in efferocytosis by regulating metabolic changes. However, future studies are required to reveal the underlying mechanisms.

5. Conclusions

In conclusion, ginsenoside Rg5 can suppress the expression of SLC7A11 and inhibit its activity via physical binding. These effects largely cancel the negative regulations of SLC7A11 on glycolysis, which fuels the efferocytosis of dendritic cells. Therefore, ginsenoside Rg5 has a potential adjuvant therapeutic reagent to support patients with wound-healing problems, such as diabetic foot ulcers.

Authorship statement

All persons who meet authorship criteria are listed as authors, and all authors certify that they have participated sufficiently in the work to take public responsibility for the content, including participation in the concept, design, analysis, writing, or revision of the manuscript. Furthermore, each author certifies that this material or similar material has not been and will not be submitted to or published in any other publication before its appearance in the *Journal of Ginseng Research*.

Declaration of competing interest

The authors declare that they have no known competing financial interests or personal relationships that could have appeared to influence the work reported in this paper.

Acknowledgements

All persons who have made substantial contributions to the work reported in the manuscript (e.g., technical help, writing and editing assistance, general support), but who do not meet the criteria for authorship, are named in the Acknowledgements and have given us their written permission to be named. If we have not included an Acknowledgements, then that indicates that we have not received substantial contributions from non-authors.

References

[1] Tapiwa Chamanga E. Clinical management of non-healing wounds. Nurs Stand 2018;32(29):48–63.
[2] Boada-Romero E, Martinez J, Heckmann BL, Green DR. The clearance of dead cells by efferocytosis. Nat Rev Mol Cell Biol 2020;21(7):398–414.
[3] Mehrotra P, Ravichandran KS. Drugging the efferocytosis process: concepts and opportunities. Nat Rev Drug Discov 2022;21(8):601–20.
[4] Khanna S, Biswas S, Shang Y, Collard E, Azad A, Kauh C, Bhasker V, Gordillo GM, Sen CK, Roy S. Macrophage dysfunction impairs resolution of inflammation in the wounds of diabetic mice. PLoS One 2010;5(3):e9539.
[5] Morioka S, Maueroder C, Ravichandran KS. Living on the edge: efferocytosis at the interface of homeostasis and pathology. Immunity 2019;50(5):1149–62.
[6] Malissen B, Tamoutounour S, Henri S. The origins and functions of dendritic cells and macrophages in the skin. Nat Rev Immunol 2014;14(6):417–28.
[7] Elizondo DM, Andargie TE, Haddock NL, Boddie TA, Lipscomb MW. Drebrin 1 in dendritic cells regulates phagocytosis and cell surface receptor expression through recycling for efficient antigen presentation. Immunology 2019;156(2):136–46.
[8] Maschalidi S, Mehrotra P, Keceli BN, De Cleene HKL, Lecomte K, Van der Cruyssen R, Janssen P, Pinney J, van Loo G, Elewaut D, et al. Targeting SLC7A11 improves efferocytosis by dendritic cells and wound healing in diabetes. Nature 2022;606(7915):776–84.
[9] Shook B, Xiao E, Kumamoto Y, Iwasaki A, Horsley V. CD301b+ macrophages are essential for effective skin wound healing. J Invest Dermatol 2016;136(9):1885–91.
[10] Phillipson M, Kubes P. The healing power of neutrophils. Trends Immunol 2019;40(7):635–47.
[11] Huang L, Cai HA, Zhang MS, Liao RY, Huang X, Hu FD. Ginsenoside Rg1 promoted the wound healing in diabetic foot ulcers via miR-489-3p/Sirt1 axis. J Pharmacol Sci 2021;147(3):271–83.
[12] Jin L, Liu J, Wang S, Zhao L, Li J. Evaluation of 20(S)-ginsenoside Rg3 loaded hydrogel for the treatment of perianal ulcer in a rat model. J Ginseng Res 2022;46(6):771–9.
[13] Lee H, Kong G, Park J, Park J. The potential inhibitory effect of ginsenoside Rh2 on mitophagy in UV-irradiated human dermal fibroblasts. J Ginseng Res 2022;46(5):646–56.
[14] Wei Y, Yang H, Zhu C, Deng J, Fan D. Hypoglycemic effect of ginsenoside Rg5 mediated partly by modulating gut microbiota dysbiosis in diabetic db/db mice. J Agric Food Chem 2020;68(18):5107–17.
[15] Zhu Y, Yang H, Deng J, Fan D. Ginsenoside Rg5 improves insulin resistance and mitochondrial biogenesis of liver via regulation of the sirt1/PGC-1alpha signaling pathway in db/db mice. J Agric Food Chem 2021;69(30):8428–39.
[16] Zhu Y, Zhu C, Yang H, Deng J, Fan D. Protective effect of ginsenoside Rg5 against kidney injury via inhibition of NLRP3 inflammasome activation and the MAPK signaling pathway in high-fat diet/streptozotocin-induced diabetic mice. Pharmacol Res 2020;155:104746.
[17] Ahn S, Siddiqi MH, Aceituno VC, Simu SY, Zhang J, Jimenez Perez ZE, Kim YJ, Yang DC. Ginsenoside Rg5:Rk1 attenuates TNF-alpha/IFN-gamma-induced production of thymus- and activation-regulated chemokine (TARC/CCL17) and LPS-induced NO production via downregulation of NF-kappaB/p38 MAPK/STAT1 signaling in human keratinocytes and macrophages. In Vitro. Cell Dev Biol Anim 2016;52(3):287–95.
[18] Wang YF, Feng JY, Zhao LN, Zhao M, Wei XF, Geng Y, et al. Aspirin triggers ferroptosis in hepatocellular carcinoma cells through restricting NF-kappaB p65-activated SLC7A11 transcription. Acta Pharmacol Sin 2023. Online ahead of print.
[19] Naik P, Sajja RK, Prasad S, Cucullo L. Effect of full flavor and denicotinized cigarettes exposure on the brain microvascular endothelium: a microarray-based gene expression study using a human immortalized BBB endothelial cell line. BMC Neurosci 2015;16:38.
[20] Lee HS, Kim MR, Park Y, Park HJ, Chang UJ, Kim SY, Suh HJ. Fermenting red ginseng enhances its safety and efficacy as a novel skin care anti-aging ingredient: in vitro and animal study. J Med Food 2012;15(11):1015–23.
[21] Van Hove L, Lecomte K, Roels J, Vandamme N, Vikkula HK, Hoorens I, Ongenae K, Hochepied T, Donati G, Saeys Y, et al. Fibrotic enzymes modulate wound-induced skin tumorigenesis. EMBO Rep 2021;22(5):e51573.
[22] Lutz MB, Kukutsch N, Ogilvie AL, Rossner S, Koch F, Romani N, Schuler G. An advanced culture method for generating large quantities of highly pure dendritic cells from mouse bone marrow. J Immunol Methods 1999;223(1):77–92.
[23] Bailey JD, Shaw A, McNeill E, Nicol T, Diotallevi M, Chuaiphichai S, Patel J, Hale A, Channon KM, Crabtree MJ. Isolation and culture of murine bone marrow-derived macrophages for nitric oxide and redox biology. Nitric Oxide 2020;100:17–29.
[24] Alam O. A single-cell-type transcriptomics map of human tissues. Nat Genet 2021;53(9):1275.
[25] Uhlen M, Fagerberg L, Hallstrom BM, Lindskog C, Oksvold P, Mardinoglu A, Sivertsson A, Kampf C, Sjostedt E, Asplund A, et al. Proteomics. Tissue-based map of the human proteome. Science 2015;347(6220):1260419.
[26] Huang QQ, Perlman H, Birkett R, Doyle R, Fang D, Haines GK, Robinson W, Datta S, Huang Z, Li QZ, et al. CD11c-mediated deletion of Flip promotes autoreactivity and inflammatory arthritis. Nat Commun 2015;6:7086.
[27] Gu Y, Albuquerque CP, Braas D, Zhang W, Villa GR, Bi J, Ikegami S, Masui K, Gini B, Yang H, et al. mTORC2 regulates amino acid metabolism in cancer by phosphorylation of the cystine-glutamate antiporter xCT. Mol Cell 2017;67(1):128–38. e7.
[28] Schappe MS, Stremska ME, Busey GW, Downs TK, Seegren PV, Mendu SK, Flegal Z, Doyle CA, Stipes EJ, Desai BN. Efferocytosis requires periphagosomal Ca(2+)-signaling and TRPM7-mediated electrical activity. Nat Commun 2022;13(1):3230.
[29] Morioka S, Perry JSA, Raymond MH, Medina CB, Zhu Y, Zhao L, Serbulea V, Onengut-Gumuscu S, Leitinger N, Kucenas S, et al. Efferocytosis induces a novel SLC program to promote glucose uptake and lactate release. Nature 2018;563(7733):714–8.
[30] Evans AL, Blackburn JW, Yin C, Heit B. Quantitative efferocytosis assays. Methods Mol Biol 2017;1519:25–41.
[31] Gerlach BD, Ampomah PB, Yurdagul Jr A, Liu C, Lauring MC, Wang X, et al. Efferocytosis induces macrophage proliferation to help resolve tissue injury. Cell Metab 2021;33(12):2445–24463 e8.
[32] Liu Y, Grimm M, Dai WT, Hou MC, Xiao ZX, Cao Y. CB-Dock: a web server for cavity detection-guided protein-ligand blind docking. Acta Pharmacol Sin 2020;41(1):138–44.
[33] Zhou C, Zhang C, Zhu H, Liu Z, Su H, Zhang X, Chen T, Zhong Y, Hu H, Xiong M, et al. Allosteric regulation of Hsp90alpha's activity by small molecules targeting the middle domain of the chaperone. iScience 2020;23(2):100857.
[34] Xia J, Ma S, Zhu X, Chen C, Zhang R, Cao Z, Chen X, Zhang L, Zhu Y, Zhang S, et al. Versatile ginsenoside Rg3 liposomes inhibit tumor metastasis by capturing circulating tumor cells and destroying metastatic niches. Sci Adv 2022;8(6):eabj1262.
[35] Poon IK, Lucas CD, Rossi AG, Ravichandran KS. Apoptotic cell clearance: basic biology and therapeutic potential. Nat Rev Immunol 2014;14(3):166–80.
[36] Liu J, Zhang X, Cheng Y, Cao X. Dendritic cell migration in inflammation and immunity. Cell Mol Immunol 2021;18(11):2461–71.
[37] Wang YZ, Xu Q, Wu W, Liu Y, Jiang Y, Cai QQ, Lv QZ, Li XY. Brain transport profiles of ginsenoside Rb(1) by glucose transporter 1: in vitro and in vivo. Front Pharmacol 2018;9:398.
[38] Gao S, Kushida H, Makino T. Ginsenosides, ingredients of the root of Panax ginseng, are not substrates but inhibitors of sodium-glucose transporter 1. J Nat Med 2017;71(1):131–8.
[39] Li S, Yu N, Xu F, Yu L, Yu Q, Fu J. Ginsenoside Rd protects cerebral endothelial cells from oxygen-glucose deprivation/reoxygenation induced pyroptosis via inhibiting SLC5A1 mediated sodium influx. J Ginseng Res 2022;46(5):700–9.
[40] Yan R, Xie E, Li Y, Li J, Zhang Y, Chi X, Hu X, Xu L, Hou T, Stockwell BR, et al. The structure of erastin-bound xCT-4F2hc complex reveals molecular mechanisms underlying erastin-induced ferroptosis. Cell Res 2022;32(7):687–90.
[41] Murphy TL, Murphy KM. Dendritic cells in cancer immunology. Cell Mol Immunol 2022;19(1):3–13.
[42] Chen P, Denniston AK, Hirani S, Hannes S, Nussenblatt RB. Role of dendritic cell subsets in immunity and their contribution to noninfectious uveitis. Surv Ophthalmol 2015;60(3):242–9.
[43] Crunkhorn S. Promoting efferocytosis heals diabetic wounds. Nat Rev Drug Discov 2022;21(7):491.

[44] Aitcheson SM, Frentiu FD, Hurn SE, Edwards K, Murray RZ. Skin wound healing: normal macrophage function and macrophage dysfunction in diabetic wounds. Molecules 2021;26(16).
[45] Bosurgi L, Cao YG, Cabeza-Cabrerizo M, Tucci A, Hughes LD, Kong Y, Weinstein JS, Licona-Limon P, Schmid ET, Pelorosso F, et al. Macrophage function in tissue repair and remodeling requires IL-4 or IL-13 with apoptotic cells. Science 2017;356(6342):1072–6.
[46] Qiang Z, Dong H, Xia Y, Chai D, Hu R, Jiang H. Nrf2 and STAT3 alleviates ferroptosis-mediated IIR-ALI by regulating SLC7A11. Oxid Med Cell Longev 2020;2020:5146982.
[47] Feng L, Zhao K, Sun L, Yin X, Zhang J, Liu C, Li B. SLC7A11 regulated by NRF2 modulates esophageal squamous cell carcinoma radiosensitivity by inhibiting ferroptosis. J Transl Med 2021;19(1):367.
[48] Feng SL, Luo HB, Cai L, Zhang J, Wang D, Chen YJ, Zhan HX, Jiang ZH, Xie Y. Ginsenoside Rg5 overcomes chemotherapeutic multidrug resistance mediated by ABCB1 transporter: in vitro and in vivo study. J Ginseng Res 2020;44(2):247–57.
[49] Yesmin Simu S, Ahn S, Castro-Aceituno V, Yang DC. Ginsenoside Rg5: rk1 exerts an anti-obesity effect on 3T3-L1 cell line by the downregulation of PPARgamma and CEBPalpha. Iran J Biotechnol 2017;15(4):252–9.
[50] Atomura R, Sanui T, Fukuda T, Tanaka U, Toyoda K, Taketomi T, Yamamichi K, Akiyama H, Nishimura F. Inhibition of Sprouty2 polarizes macrophages toward an M2 phenotype by stimulation with interferon gamma and Porphyromonas gingivalis lipopolysaccharide. Immun Inflamm Dis 2016;4(1):98–110.